Optimizing the range of a bilateral filter to enhance defects and threads visibility in X-Ray radiographic testing

T. Madmad[a], V. Libertiaux[b], and C. De Vleeschouwer[c]

[a,c]UCLouvain, ICTEAM, Louvain-La-Neuve, Belgium
[b]ULiège, Univerity of Liège, Belgium

ABSTRACT

Radiographic testing is extensively used in non-destructive evaluation. However, the contrast of object defects in X-Ray images is generally weak compared to the image dynamic range, which limits defects visibility and makes the image inspection time consuming and tedious. To circumvent this issue, our work builds on a bilateral filter to extract and amplify the low-contrast local variations of the image, supposed to represent the object defects. A critical step of this approach lies in the selection of the bilateral filter range parameter, which sets a contrast upper-bound to the signals that are filtered out, to be scaled to a constant fraction of the rendering range. As an original contribution, we propose to set this parameter to maximize the tone-mapped quality index (TMQI) of the reconstructed image. Since the TMQI combines a multi-scale structural similarity criterion with a measure of image naturalness, its maximization both discourages the selection of a (too large) range parameter that penalizes structural similarity, and prevents the lack of naturalness associated to an excessive noise amplification caused by a too small range parameter. Image subjective quality assessment experiments not only demonstrate that our approach largely enhances defect visibility on real use cases, but also reveal that our recommended parameter is preferred by users to any reasonable alternative in a large majority of cases (90%). An objective evaluation based on the Image Discrete Entropy shows that the enhanced images compare favorably to the ones obtained with previous works devoted to High Dynamic Range image visualization.

Keywords: Defect and threads highlighting, local contrast enhancement, X-Ray radiographic testing, Non-destructive evaluation

1. INTRODUCTION

X-Ray radiographic testing (RT) have been used as one of the main tools for non-destructive evaluation of materials in various industrial applications. This is because X-rays offer the possibility to visualize inside material imperfections in a non-invasive manner. In fact, radiography consists in directing radiation from an X-Ray generator through the material under inspection. The radiation is then attenuated by the object, before being captured by detectors and converted by dedicated readers into image intensities. As a result, when a local loss or gain in the material density is introduced inside the object during the manufacturing process, it systematically leads to a local intensity variation in the captured X-Ray image. Those local and fine variations usually represent the defects and the object imperfections. These intensity variations can be collected without opening or destroying the object which explains the popularity of RT in non-destructive testing and evaluation. In the aerospace domain, X-Ray radiographic testing is used to identify the presence of defects in aircraft wings,[1] in the electronic domain it is used to check the integrated circuits and chip modules.[2,3] X-Ray non-destructive testing is also used for security and cargo checking.[4–6]

The practical usability of X-ray RT is however conditioned to the appropriate visualization of X-Ray images. This question is not trivial since those images are characterized by a High Dynamic Range (HDR) of their intensity levels. Those levels reflect the X-Ray absorption power of the observed object.[7] Hence, a wide range of intensities is required to simultaneously capture the large absorption discrepancies observed in a scene (between

Send correspondence to :
T. Madmad: E-mail: tahani.madmad@uclouvain.be

high density objects and X-Ray transparent ones) and the small variations of X-Ray absorption induced by the object surface texture or defects and threads such as cracks in metal, welding imperfections or composite inclusion.

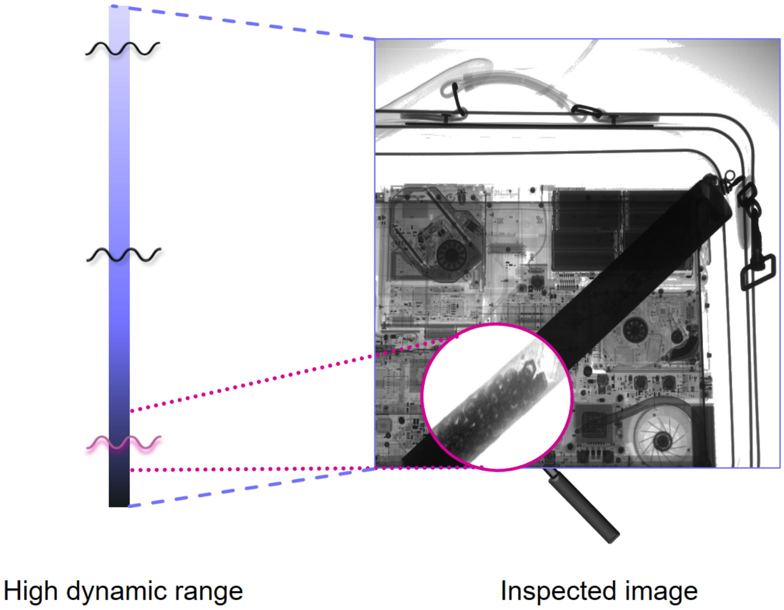

Figure 1: The image represents a tricked out luggage. The X-Ray defects corresponds to the nails contained in a steel tube. The threads are not perceivable when the X-ray intensity levels are linearly mapped to the image intensities. A local stretching allows to visualize the hidden prohibited item when inspecting the luggage image part by part.

In X-Ray RT systems, images have a dynamic range that exceeds by far the intensity range available on the screen. Even though several manufacturers offer new display systems with higher bit depth,[8] the perception of the image signals by the operator is itself limited by the human visual system capabilities: the number of gray levels that an average user can perceive as distinct is indeed limited to around 1000 levels of distinguishable intensities for experts (measured in JND).[8] Typically, X-Ray images that are recorded with 16 bits depth per pixel or more, corresponds to 65536 possible intensity levels per pixel,[9] whereas the range of intensities visible and distinguishable at once by the human eye in optimal conditions corresponds to 9 bits depth images only. Therefore, a monitor offering an intensity range equivalent to the dynamic range of the image is not enough to make the weakly contrasted image structures visually perceptible.

This problem is especially critical regarding the perception of defects, which are characterized by a weak contrast compared to the X-Ray image intensity range. This weak contrast limits their visibility and makes the inspection of the various objects time consuming and tedious. To circumvent this issue, image processing methods are deployed as a core image enhancement instrument in the NDT & E chains. Typically, image contrast enhancement and sharpness improvement algorithms have been widely investigated[10] but still, the developed frameworks are usually specific to a restrictive domain of radiographic testing. At the same time, the rapid growth of technology has facilitated the development of portable and versatile X-Ray systems for non destructive testing (RT), thereby broadening the kinds of content observed by the same device. Under such circumstances, content-dependent approaches are no longer sufficient for recent RT inspection systems and universal solutions that are able to adapt to various image content should be considered as a key tool to support the technological development of NDT & E systems. Our paper leverages on the well-known bilateral filter to enhance the contrast of image defects in arbitrary X-ray images. The practical use of this filter requires to select a parameter, named range parameter, to set a contrast upper-bound to the signals that are filtered out, to be scaled to a constant fraction of the rendering range. As an original contribution, our work proposes to select the range parameter to maximize the tone-mapped quality index (TMQI)[11] of the reconstructed image. Since the TMQI combines a multi-scale structural similarity criterion with a measure of image naturalness, its maximization both discourages the selection of a (too large) range parameter that penalizes structural similarity, and prevents the lack of naturalness associated to an excessive noise amplification caused by a too small range parameter.

The rest of our paper is organized as follows. Section 2 briefly surveys the related works associated to X-Ray images visualization and local contrast enhancement, in addition to image quality assessment methods for HDR content. Section 3 provides a formal description of our proposed method. Experimental validation is presented in Section 4.1.1. Section 5 concludes .

2. RELATED WORKS

Enhancing the visualization of images is one of the most fundamental research fields in image processing to extract meaningful and useful content and features for high-level tasks such as medical diagnosis, components testing, luggage checking, work of art authenticity inspection and various other areas of NDT & E. Although technological advances have greatly improved the visualization of HDR images, X-Ray radiographic images generally suffer from weekly-contrasted local structures including defects and threads. This intrinsic trademark of digital X-Ray (and more generally high dynamic range) imaging systems affects seriously the smoothness of the inspection process in radiographic testing applications. In this context, various image enhancement methods have been suggested in the literature to tackle the low local contrast of semantically meaningful structures in HDR and X-Ray imaging. Those methods can be separated into two main categories: (i) histogram-based methods, and (ii) filtering-based methods.

2.1 Histogram-based methods

Histogram Equalization (HE) regularizes the image histogram to achieve better visualization results. The main idea of HE is to stretch the image histogram according to the occurrence of intensities in the image. To better exploit the rendering range in each region of the image, Pizer et al.[12] proposed an Adaptive Histogram Equalization (AHE) that calculates the local distribution based on a sliding window. Although this type of local approaches are successful in improving the local contrast of the images, they suffer from a high computational time and generally introduce global inconsistency, brightness migration and over-enhancement in the image.[13] To circumvent this issue, Zuiderveld[14] proposed an improved algorithm called Contrast Limited Adaptive Histogram Equalization (CLAHE) inspired from.[12] CLAHE is an amplitude clipping method that tackles the problem of local over-enhancement by clipping and redistributing the histogram gray peaks before applying HE. CLAHE and its variants[15–17] have been applied to various digital X-Ray radiography domains.[18,19] Despite histogram-clipping strategies have good performances when it comes to image contrast and visualization improvement, their main drawback remains the selection of several important parameters including the contrast limit and the window size to achieve optimal results. Therefore, adopting such strategies as an enhanced visualization process, implicitly means a time-consuming trial-and-error process to set the method parameters for each X-Ray image, which makes it inappropriate for X-Ray radiographic testing application.

2.2 Filtering-based methods

Filtering-based strategies for image-contrast enhancement have been deployed as an efficient tool in various visualization applications.[20–22] Historically, those methods have been developed to take the spatial distribution of intensities into account when enhancing the images, unlike histogram-based strategies that only takes into account the intensity occurrences. Linear filters, such as the Gaussian filter,[23] treat the pixels independently of the image content. It follows that sharp image edges and weakly contrasted defects are filtered in a similar manner, making linear filters inappropriate to isolate (and amplify) defects structures in an image. To overcome the drawbacks of linear filters, filters whose coefficients are weighted based on the local image content were proposed in the literature. For instance, the anisotropic filter[24] evaluates the gradient to guide the image filtering process. The bilateral filter[25] averages neighboring pixels with weights/coefficients that depend on two main information : the spatial and the intensity distance. The cross-bilateral filter[26] extends the bilateral filter principle by using an additional input, named guidance image, to define the intensity distance considered in the filter coefficient definition. In this context,[27] introduce the bilateral histogram equalization and offers a good balance between global and local tone-mapping by adapting the mapping locally based on the global distribution of intensities but yet it is time consuming and can introduce some ringing artefacts in some special cases as explained in.[27] Heet al.[28] introduced the guided image filter, which behaves similarly to the bilateral filter, but at smaller computational complexity and prevents the unwanted gradient reversal artifacts that might occur with bilateral filters. This method was successfully applied in tasks such as image dehazing and super resolution. In this work, we propose a locally adaptive framework for X-Ray radiography NDT & E that aims to highlight threads and defect based on a bilateral filtering strategy.

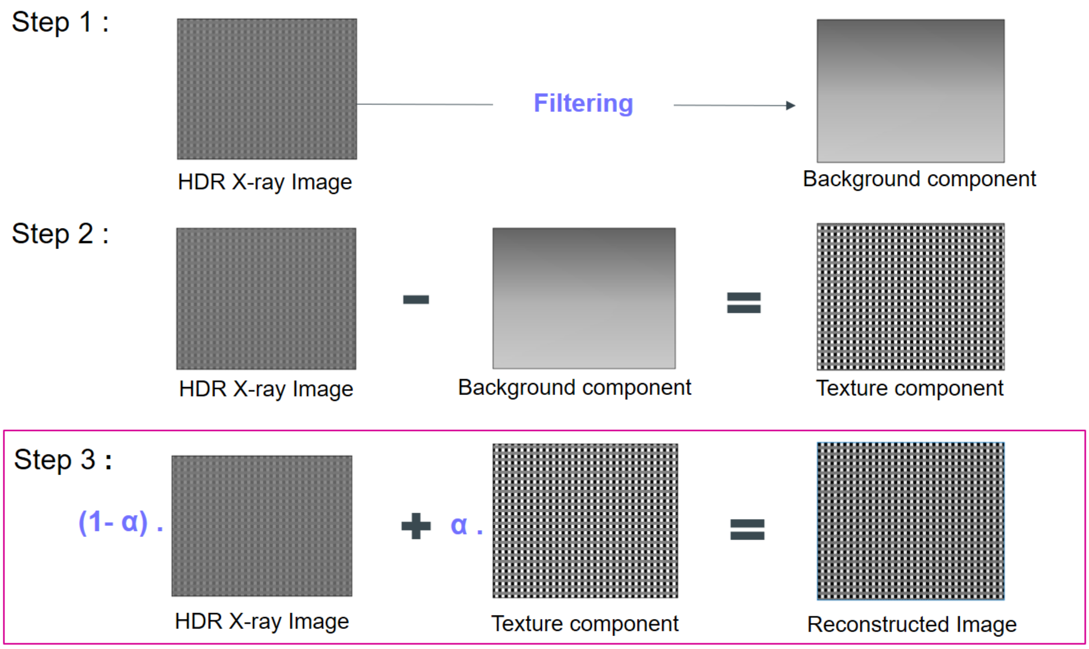

Figure 2: Step by step illustration of our defects and threads visibility enhancement approach. Each row represent one step of our method. The first step consists on smoothing the original image. The second step of our method mainly extract the residual component. The last step of our approach aims to reconstruct the inspected image by amplifying the residual component containing the defects and threads.

3. DEFECTS AND THREADS VISIBILITY ENHANCEMENT FOR X-RAY RADIOGRAPHIC TESTING IMAGES

The global framework of our bilateral filtering-based strategy for defects and threads highlighting builds on few assumptions and hypothesis. Inspired by the image morphological decomposition frameworks,[29,30] we assume that an X-Ray image can be decomposed into two main components corresponding to distinct and meaningful classes of signals. Furthermore, we assume that the signal describing the threads and the defects sought meets the following characteristics:(i) Mathematically singular and rarely represented in the image,(ii)Structured unlike the electronic noise signal for example.(iii)Weekly contrasted due to a slightly increase or decrease of the intensity value compared to the background.

In this Section, we first introduce the bilateral filtering-based approach for defects and threads visibility enhancement in X-Ray RT images. As an original contribution, we explain in the last part of this Section, how the range parameter of the bilateral filter can be optimized and set in an adaptive manner, making this method universal and compatible with several applications of RT techniques.

3.1 Divide and conquer: our overall framework

Our method is based on two main steps : divide and conquer.

3.1.1 Divide : X-Ray images decomposition for NDT & E

The first step consists in the decomposition of the original X-Ray image into two distinct classes of signals :

1. **The background component:** This component is defined as the piece-wise smooth variations of the X-Ray image intensity values and it can be compared to a cartoon image. Physically speaking, it represents the average power of the examined objects to absorb X-Rays and it is proportional to the object's density and depth. The background component is obtained by filtering the original input image with a bilateral filter.

2. **The residual component:** This component corresponds to the fine variations of the X-Ray image intensity values that usually contain meaningful and structured singularities of the signal including the defects and threads. The residual component is obtained by subtracting the background component from the original input image. It contains the weakly contrasted structures, but also the noise in the image.

3.1.2 Conquer : X-Ray images visibility enhancement for NDT & E

The second step "conquer" consists of enhancing the visibility of defects and threads by combining the residual component and the input image based on a weighted sum. The weight factor α assigned to the residual component controls the amplification of this component compared to the background. By tuning the parameter α, the users are given the opportunity to control the contribution of each new component to the final reconstructed image. This option is very useful and effective in practical non-destructive testing use cases. In fact, this gives the possibility to the RT operators to return back to the original view of the X-Ray image, view only the extracted threads or combine both and highlight the defects simply by moving a slider that changes the value of α. As this process consists on a simple adjustment of the residual component weight, the computation cost remains low, which make this operation completely compatible with real time applications.The reconstructed image I_{rec} is defined as a weighted sum of the background and residual images. Formally, the background and residual image are first normalized. It means that, for each image, the intensities are linearly transformed so that the image histogram covers the entire rendering dynamic range. The normalized background and residual images, respectively named I_b and I_r, are then combined to define the reconstructed image I_{rec} as:

$$I_{rec} = (1-\alpha) \cdot I_b + \alpha \cdot I_r, \text{ with } \alpha \in [0,1]. \tag{1}$$

Hence, α can be interpreted as the fraction of the rendering dynamic range devoted to the residual image.

The most crucial aspect of our approach lies in the choice of the filter to be applied to the original image. As we intend to amplify the image components that represents defects and threads, the main trade-off is how to define the filtering operation so as to filter out only the interesting structures such as cracks and inclusions without filtering out (and thus including in the residual component) the large edges of the image. In fact, the drawback of filtering the large edges of the image, would be that the residual component would contain not

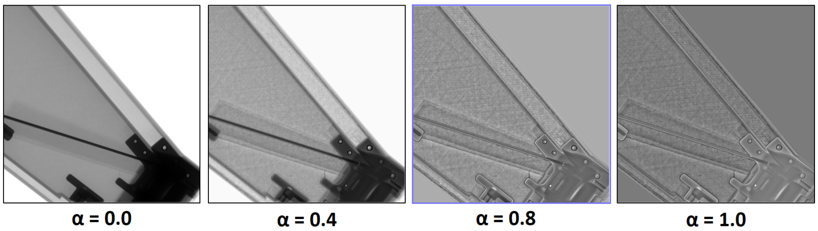

Figure 3: Reconstruction of the image I_{rec} using different values of α. The range parameter and the spatial parameter are fixed. Interestingly, by tuning the parameter α our method offers the end-user the opportunity to evolves progressively from the visualization of the absorptive power variations rendered by a linear mapping ($\alpha = 0$), to the observation of the fine textural and structural object details ($\alpha = 1$).

only the defects to highlight but also the large steps of intensities associated to regular image edges. Consequently, the amplification of the residues would be limited to a factor maintaining the amplification of large edges within the rendering dynamic range. In the next part of this Section we discuss the filtering strategies and explain why the bilateral filter is appropriate to isolate the defects without filtering out the large edges in the image.

3.2 Bilateral filtering

To limit the inclusion of regular image structures in the residual, our work proposes to compute the background component based on an edge-preserving filter. The guided filter[31] and the bilateral filter[26,32] are two perfect candidates for this purpose. To mitigate the computation costs, we recommend the use of the fast bilateral filter version.

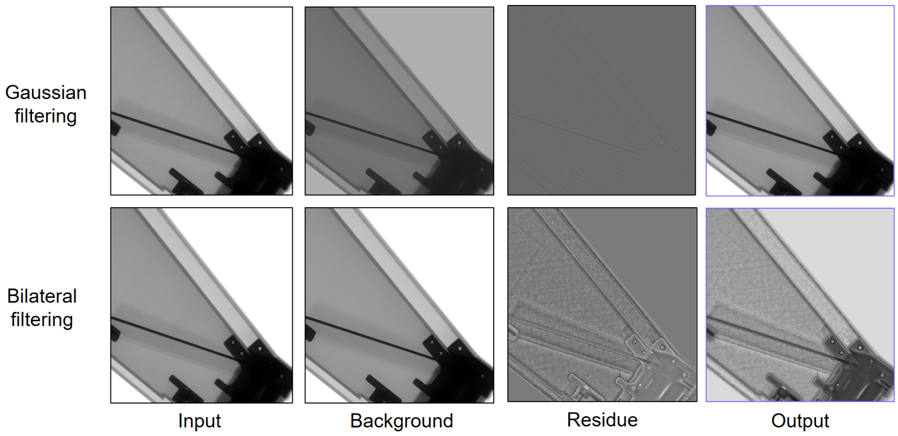

Figure 4: Comparison between the Gaussian filtering strategy (Top row) and the Bilateral filtering strategy (Bottom row). The reconstruction parameter and the spatial parameter being fixed.

The bilateral filter formulation is simple and each pixel is replaced by the average of its neighbors. This is an interesting aspect because it makes it easy to acquire intuition about the filter's behavior. In this way, adapting the bilateral filter to specific applications does not require complicated analysis.[33] In order to smooth the input image while still tolerating the preservation of sharp regular edges, the bilateral filter replaces, the central pixel value by an average of the intensity values over the chosen neighborhood of pixels. The originality of the bilateral filter compared to a conventional Gaussian filter lies in the definition of the weights given to each neighboring pixel value. Two main aspects are considered to define those weights: the spatial distance, and (this is a specificity) the tonal distance. To clarify, the more the neighboring pixels are distant from the central position of the filter, the lower is their corresponding weights and thus their contribution to the final value of that pixel. Similarly, the more the neighboring intensities are contrasted compared to the central pixel value (which means that they probably belong to different piece-wise smooth portion of the scene), the weakest are their weights and thus their contribution to the final value computed by the filter. Formally, the intensity and the spatial distance aspects are managed by distinct Gaussian.

Mathematically, the original image I is filtered to provide the bilateral filtered background $I_b(x,y)$ as follows:

$$I_b(x,y) = \kappa^{-1}(x,y) \cdot \sum_{(p,q)\in\Omega(x,y)} I(p,q) \cdot G_{\sigma_r}(||I(p,q) - I(x,y)||) \cdot G_{\sigma_s}(||(p,q) - (x,y)||). \tag{2}$$

with $\Omega(x,y)$ defining a spatial neighborhood centred in the pixel coordinate (x,y), $G_{\sigma_r}(x) = \exp\frac{x^2}{2\sigma_r^2}$ being the Gaussian range kernel, and $\kappa(x,y) = \sum_{(p,q)\in\Omega(x,y)} G_{\sigma_s}(||(p,q)-(x,y)||) \cdot G_{\sigma_r}(||I(p,q) - I(x,y)||)$ being the normalization constant.

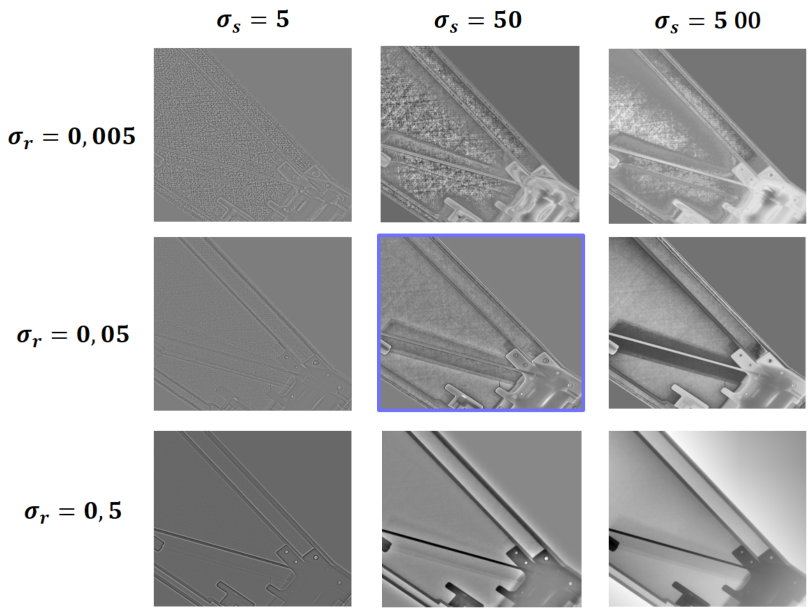

Figure 5: The impact of the range parameter σ_r and the spatial parameter σ_s on the extraction of the residual component. The reconstruction parameter is fixed.

The bilateral filter has two main parameters:σ_s and σ_r. The Figure 5 illustrates the impact of each parameter on the extracted residue. Small σ_s values promote the inclusion of thin structures in the residual image. In practice, we recommend to set σ_s to the expected maximal thickness of the defects to enhance in the context of interest.

3.3 Which range parameter is the best for defects and threads visibility enhancement in NDT & E ?

Reducing the value of σ_r reduces the weight and impact of the neighboring pixels that differ from the central pixels. Hence, it results in a background that is quite similar to the initial image, and in a residual image that only includes the small and local variations of intensities. As a consequence, a too small $\sigma_r$only includes noise in the residual. A too large σ_r ends up in including highly contrasted regular image structures in the residual, which limits the factor by which the defects of interest are amplified (since a constant dynamic range is assigned to the residual in the reconstructed image). The spatial parameter σ_s defines the size of the structures to be kept by the filter and it is usually fixed as a function of the input image shape.

As an original contribution, we suggest to select σ_r optimal value by maximizing a meaningful image quality metric between the reconstructed LDR image and its corresponding initial image. This quality metric has been selected as a metric that is penalized when the reconstructed image (1) presents noisy patterns, or (2) differs from the initial image in terms of key structures. Those two characteristics ensure that maximizing the quality metric will avoid selecting a too small (which adds noise) or too large (which affects the key structures) σ_r. The TMQI metric provides the required characteristics.

The TMQI is defined as a combination of two main terms inspired from two different IQA models. The first term of the TMQI is based on the Structural Similarity Index Metric (SSIM) in its multi-scale version.[34] This part mainly aims to encourage the structural similarity between the two images taken as input. The second term of the TMQI is similar to on a Natural Scene Statistics (NSS),[35] which compares the assessed image statistics to those made on natural images.[36] The aim of this second part of the TMQI is to penalize the cases where the signal variations are significant in one of the image local patches but insignificant in the other. This is typically the case of unnatural images where for example the noise has been amplified in an excessive manner.

Formally, the TMQI score Q comparing the original image to the reconstructed image is defined as follows :

$$Q = a \cdot S^{\alpha} + (1-a) \cdot N^{\beta}. \tag{3}$$

where S and N are the multi-scale structural similarity and the naturalness components respectively. The parameter $0 \leq a \leq 1$ allows to adjust the respective weights (importance) of these components. α and β determine their respective sensitivities. Since both S and N are upper-bounded by 1, the overall quality measure is also upper-bounded by 1.[36]

3.3.1 The multi-scale structural fidelity

The statistical naturalness component is defined Let u and v be two local image patches extracted from the original X-ray image and the reconstructed images respectively. The TMQI defines the local structural fidelity measure as follows :

$$S_{local}(u,v) = \frac{2 \cdot \sigma_u^{'} \cdot \sigma_v^{'} + \epsilon_1}{\sigma_u^{'2} + \sigma_v^{'2} + \epsilon_1} \cdot \frac{\sigma_{uv} + \epsilon_2}{\sigma_u \cdot \sigma_v + \epsilon_2}. \tag{4}$$

where σ_u , σ_v and $\sigma_u v$ are the local standard deviations and the cross-correlation between x and y. ϵ_1 and ϵ_2 are positive stabilizing constants. $\sigma_u^{'}$ and $\sigma_v^{'}$ are the reconstructed versions of $\sigma_u^{'}$ and $\sigma_v^{'}$, respectively as explained in.[36] They are bounded between 0 and 1.

The local structural fidelity map S_{local} is generated at multiple scales and the multi-scale structural fidelity is defined as follows:

$$S_l = \frac{1}{N_l} \sum_{i=1}^{N_l} S_{local}(u_i, v_i). \tag{5}$$

Where L is the total number of scales. N_l being defined as the number of patches in the l-th scale level. $u_i and v_i$ are the i-th patches extracted from the original and reconstructed images respectively, for comparison purposes.

The overall structural fidelity S is defined by the TMQI as the combination of different scale levels of the local structural fidelity scores,[36] and it is formally defined as follows:

$$S = \prod_{l=1}^{L} S_l^{\beta_l}. \tag{6}$$

where β_l is the weight corresponding to the $l - th$ scale.

3.3.2 The local statistical naturalness

The statistical naturalness model of the TMQI is based on the statistics conducted on many different types of natural scenes. The key observation is that the histograms of the means and standard deviations of natural images fit a Gaussian and a Beta probability density functions.[36] The TMQI is based on their joint probability density function and thus defines the statistical naturalness score N as follows :

$$N = \frac{1}{K} \cdot P_m \cdot P_d. \tag{7}$$

where P_m is the Gaussian probability density function and P_d being the Beta probability density function. K is a normalization factor given by $K = \max(P_m, P_d)$.

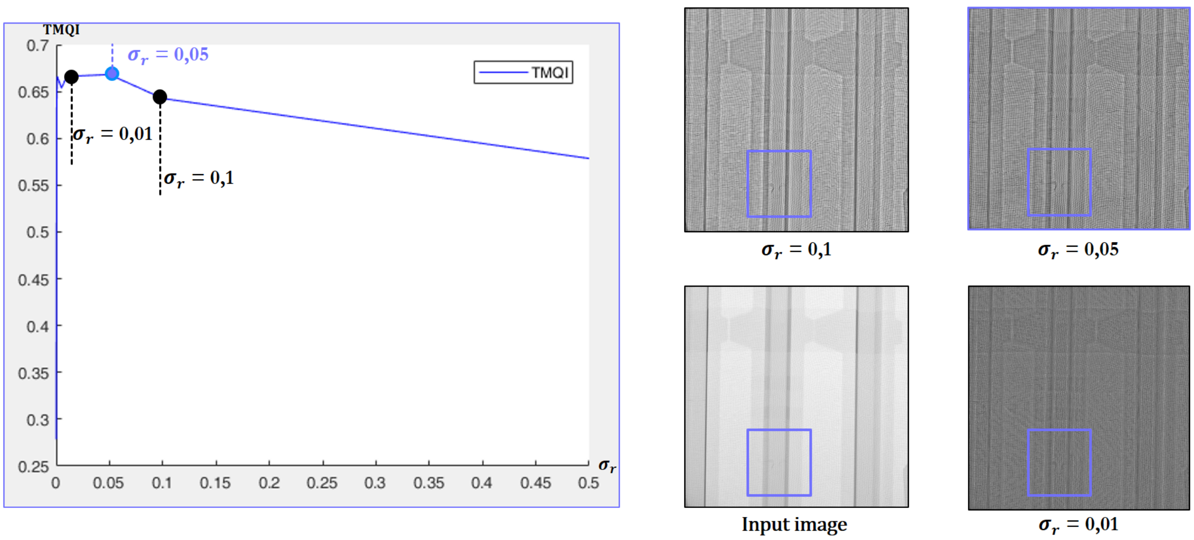

Figure 6: Range parameter selection process. The curve represented in the left part of the Figure shows the suggested value $\sigma_r = 0.05$ that maximizes the TMQI[11] and its neighboring values $\sigma_r = 0.1 and \sigma_r = 0.01$. The reconstruction parameter and the spatial parameter are fixed.The original image and the images generated using each of these values are shown in the right part of the Figure.

Typically, the TMQI score prevents in one hand the lack of naturalness associated to too small values of the range parameter, and in the other hand it discourage the penalization of the structural similarity associated with too large values of σ_r.

The value of the bilateral filter range parameter σ_r^* that optimizes the defects and threads visibility enhancement in X-Ray NDT & E is defined as follows :

$$\sigma_r^* = \arg\max_{\sigma_r}(Q(\sigma_r)). \tag{8}$$

The Figure 6 shows how the maximum value of the TMQI enables to select the range parameter that results in best visibility of the features of interest. The reconstructed images from non optimal range parameters shows that the choice of the range parameter is very decisive. To compare the impact of the range parameter on the reconstructed image without any bias, we fixed all the other parameters. The Figure 6 also illustrates how small variations of σ_r leads to a significant change in terms of the visibility of the defect and threads in the reconstructed image.

4. EXPERIMENT AND RESULTS

In this Section,both subjective and objective image quality assessment (IQA) procedures are considered. For each kind of assessment we describe the global layout and the parameter setting of the validation experiment before presenting their corresponding results. The first experiment is a benchmark process where the images reconstructed based on our method are compared to the images processed by well-known HDR image visibility enhancement methods destined for HDR images.[25,37–39] The second experiment aims to qualitatively compare the visibility of threads and defects when reconstructing the images with our method, but using different σ_r parameters (including our recommended value, i.e. the value maximizing TMQI). Both of the experiments are conducted on X-ray images that emanate from real life application in NDT&E including archaeological objects, plastic based component, welds, casting pieces and security domains objects. Moreover, different use cases are considered in order to analyze the performance and the universality of the suggested method.

4.1 Assessing the σ_r selection based on a subjective perceptual experiment

4.1.1 Experimental procedure

The subjective image quality assessment experiment involved 35 participants. Even if the users are not X-ray image or NDT & E experts, most of them work as researchers within the image and signal processing domains.

Before starting the test, the users are shown synthetic X-ray images representing inspected objects with typical NDT & E defects such as fractures or inclusions like shown by the Figure 7 (a). This is a preliminary step to make sure the users understand that the goal of our method is to enhance the visibility of defects for inspection purposes. During the test experiment, all the test questions are configured as forced choice tests, where the users are forced to select one of the two options proposed as possible answer. For each question, the original X-ray image is displayed with two of its reconstructed versions, and the viewer has to select her preferred reconstructed image. The procedure is presented in Figure 7 (b). No time limit is imposed to the viewer to make her choice.

4.1.2 Parameter setting

Our proposed method, involves three main parameters, namely the range parameter σ_r, the spatial parameter σ_s , in addition to the reconstruction parameter α that defines the fraction of the rendering range devoted to the residual signal. In this Section, σ_s is set to 10% of the image size, and α is set to 0.07. Our goal is to study the impact of σ_r. The recommended value of the range parameter σ_r, which maximizes the TMQI between the input X-ray image and the reconstructed image , is compared to alternative choices, including the default values of the TMQI parameters as proposed by.[36] The bilateral filter is implemented as in,[36] using the algorithm developed by.[36]

4.1.3 Dataset generation

We consider ten different original test X-ray images displaying objects from various application in NDT & E. More precisely, we consider two different images from each of the following applicative domains: i) Ceramic pieces, ii) Composite pieces, iii) Plastic objects, iv) Archaeological objects and v) Welds. Three reconstructions of each original image are generated using distinct values of the bilateral filter range parameter σ_r. In practice, for each test image, given the value σ_r^* that maximizes the reconstructed image TMQI, the three values of σ_r

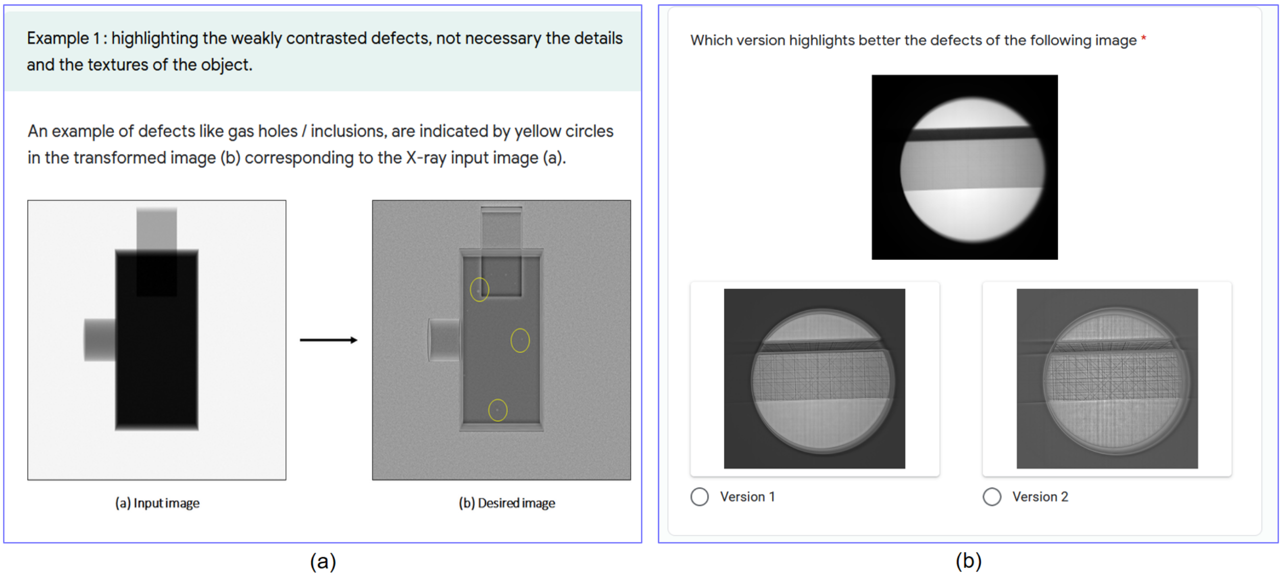

Figure 7: (a) Test question sample. The viewer has to select among two reconstructed versions of a same original image, presented in the center of the screen. (b) Illustration of defects. Those illustrations are presented to viewers before they start the actual test, so that they understand what is the purpose of the visualization, and thus image enhancement, process.

adopted in our subjective experiment are $\sigma_r^* - 0.05$, σ_r^*, and $\sigma_r^* + 0.05$.

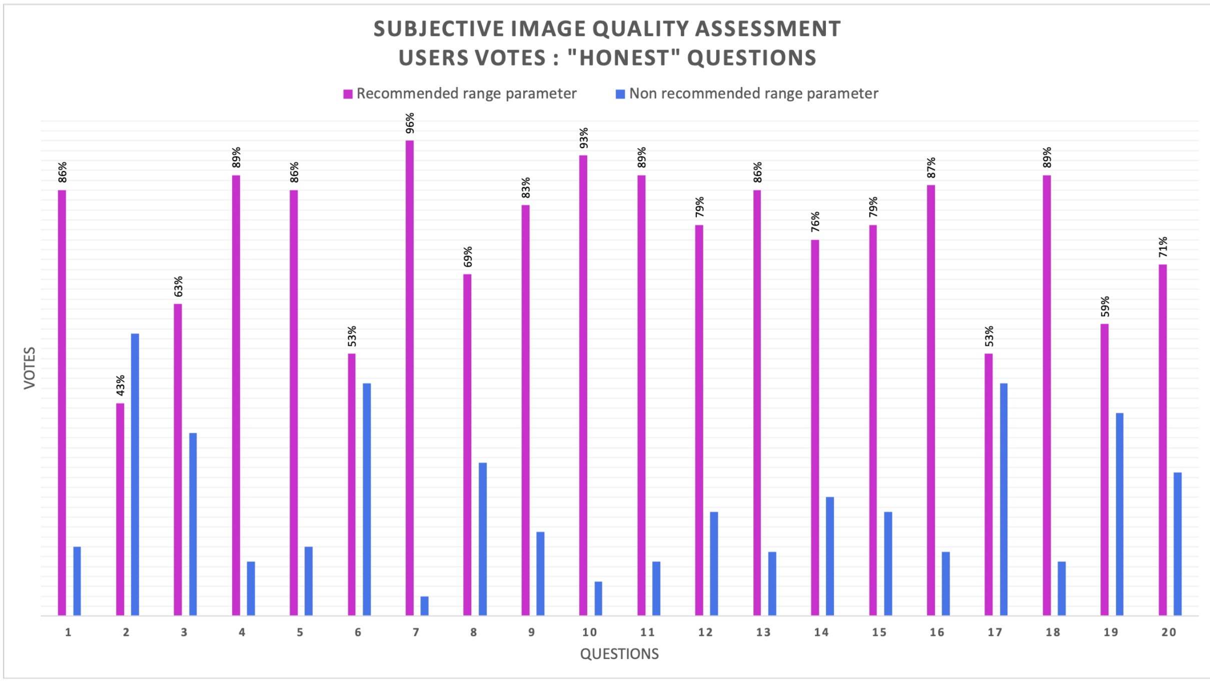

Figure 8: Subjective assessment. The plot depicts the percentage of viewers who have selected the recommended σ_r, when it is compared to a (slightly) smaller or larger σ_r. We observe that the recommended value is preferred in more than 90% of cases.

4.1.4 Test configuration

In order to validate the proposed setting of the bilateral filter range parameter for threads and defects visibility enhancement in NDT & E, we combine two types of test questions : ”honest” questions and ”tricky” questions. When a ”honest” question is asked, users are shown in addition to the original X-ray image, one optimal and one non optimal image. We mean by optimal image, the image generated using σ_r^*. the non optimal image is either generated by setting σ_r to $\sigma_r^* - 0.05$, or $\sigma_r^* + 0.05$. When it comes to a ”tricky” question, both of the images shown to the users in addition to the original X-ray image,are non optimal images. In other words, the ”tricky” choices are generated by setting $\sigma_r^* - 0.05$ and $\sigma_r^* + 0.05$ only.

4.1.5 Experiment results

The results of the subjective image quality evaluation are illustrated in the Figures 8 and 9. The graphic shown in Figure 8 gives an overview of the user votes to the ”honest” questions. For instance, there are 20 questions (60%) among the test experiment where users are asked to choose between the version of the image generated based on the optimal range parameter σ_r^* the one generated by considering an immediate neighboring value of σ_r^*. As it can be seen in Figure 8, in 95% of the cases the optimal range parameter outweighs the non-optimal one in terms of votes. Moreover, one can clearly spot a general tendency in favor of the optimal parameter since, our recommended σ_r value is preferred by the great majority of users. In contrast, the votes on ”tricky” questions does not reveal a specific preference. As shown in Figure 9, for 90% of the ”tricky” questions (9/10), the weights of the competition images are close to each other and none of the images collected more than 60% of the users votes. This is an interesting result since it confirms that users may make random choices when there is no optimal image which explains the difference with the 8.

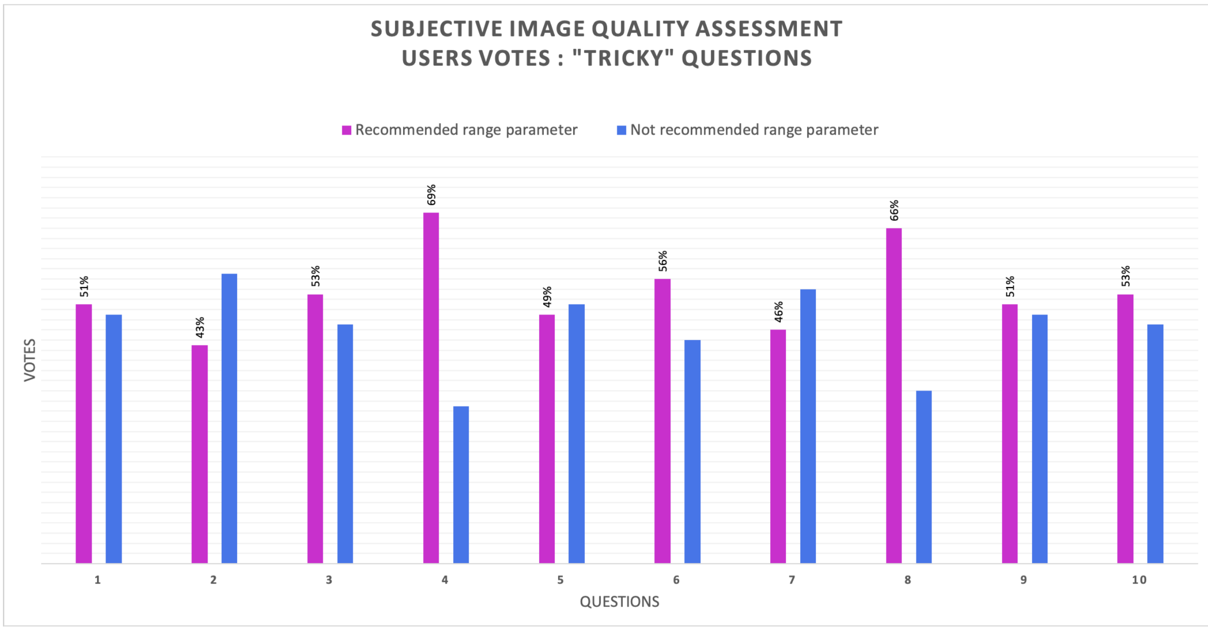

Figure 9: Subjective assessment. the graph illustrates the users votes to the ”tricky” questions. We observe that for 90% of the cases, it is difficult to decide if the general tendency is in favor of one of the viewed images.

4.2 Comparison with SoA, using visual and objective image quality assessment

In order to assess the objective image quality of our method, we conduct a benchmark study where we compare our resulted images with images processed by the state of the art method.[25,37–39] More precisely, we consider six NDT & E images coming from distinct domains respectively and we compare the results in each case based on two main objective metrics namely the Image Discrete Entropy and the Feature Structured Similarity Index

Measure (FSSIM).[40] Figure 10 illustrate the processed X-ray images of six different workpieces that emanates from different domains. We compare our results qualitatively to the well known state of the art methods. The tables 1 and 2 shows how our method compares favorably to classical approaches where the parameter setting is pre-fixed independently on the image content.

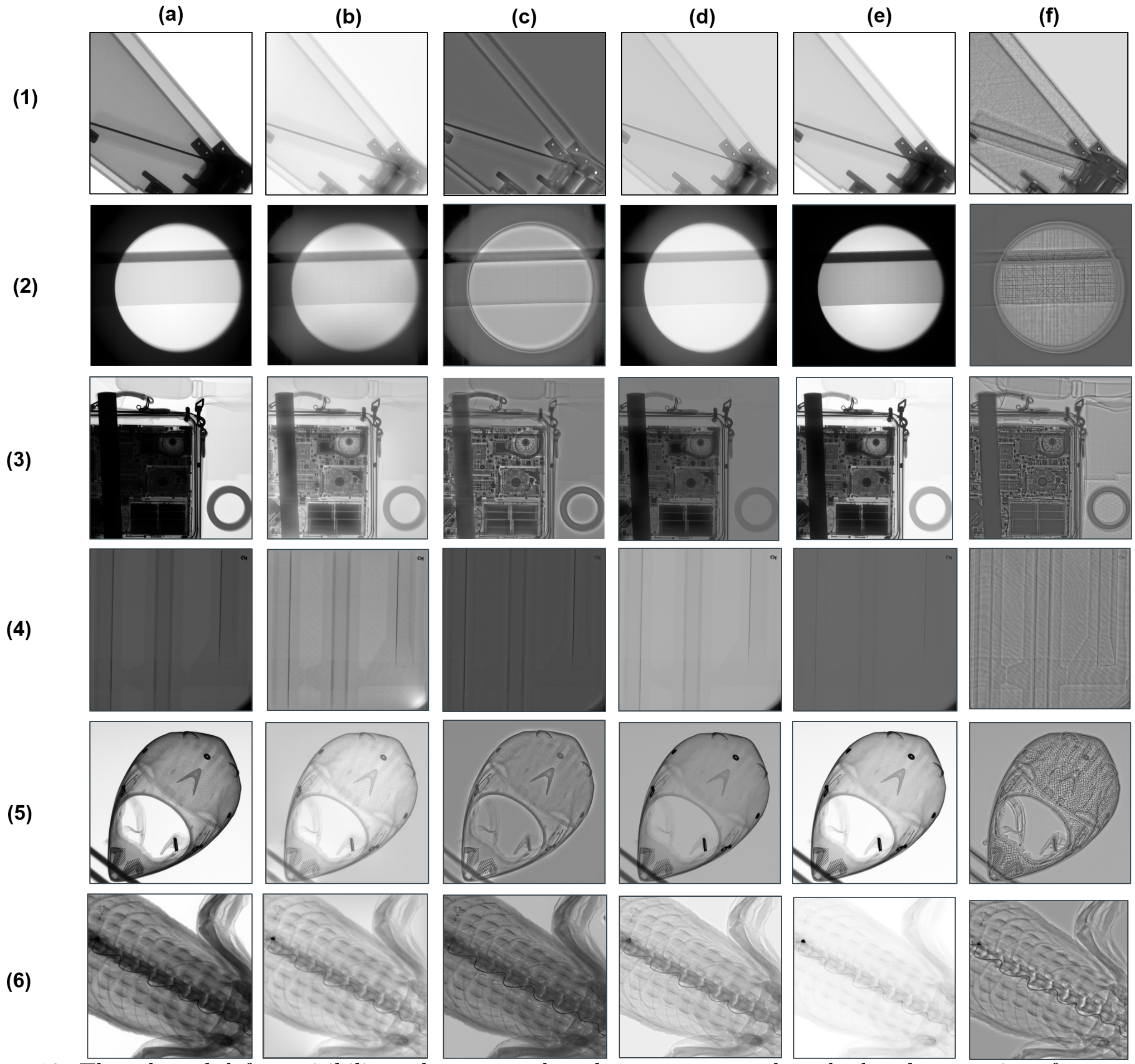

Figure 10: Threads and defects visibility enhancement based on our proposed method and comparison for a set of 6 X-ray HDR images that emanate from various domains : (1) composite industrial forks , (2) composite aviation parts, (3) security domain object, (4) casting pieces, (5) plastic object, (6) archaeological object. For all the images (rows from (1) to (6)), we show the corresponding processed images. (a) Original. (b) Fattal,[37] (c) Durand,[25] (d) Ashikhmin,[38] (e) Reinhard,[39] (f) ours. The images of the benchmark study are generated with a fixed α value (0.7).

	(1)	**(2)**	**(3)**	**(4)**	**(5)**	**(6)**
Input (reference)	0.540	0.005	0.951	0.980	0.984	0.777
Fattal[37]	0.040	0.089	0.283	0.953	0.780	0.077
Durand[25]	0.561	0.005	0.304	0.982	0.693	0.718
Ashikhmin[38]	0.335	0.029	0.534	0.002	0.010	0.538
Reinhard[39]	0.509	0.005	**0.985**	**0.998**	**0,997**	0.906
Ours	**0.607**	**0.995**	0.967	0.980	0.991	**0.984**

Table 1: Objective quality assessment results based on the Image Discrete Entropy measure

	(1)	**(2)**	**(3)**	**(4)**	**(5)**	**(6)**
Fattal[37]	0.770	0.808	0.749	0.794	0.565	0.625
Durand[25]	0.898	0.948	0.916	0.891	0.926	0.942
Ashikhmin[38]	0.803	0.850	0.799	0.853	0.682	0.625
Reinhard[39]	0.759	0.861	0.682	0.791	0.555	0.518
Ours	**0.924**	**0.986**	**0.941**	**0.925**	**0.955**	**0.953**

Table 2: Objective quality assessment results based on the FSSIM[40]

Due to the limitation of the dynamic range, few details can be readily perceived in the input image. We consider 4 main tone mapping algorithms destined for HDR images visualization. As shown by the Figure 10 the images processed by the state of the art methods still suffer from weekly contrasted defects and threads. More specifically, the overall brightness of the images resulted from Fattal's,[37] Ashikhmin's[38] and Reinhard's[39] algorithms is indeed improved and some of the fine structures and details are highlighted to some extent. But the disadvantages are also obvious: the images appear to be bright but the contrast of the defects and threads is not enough to spot them easily. In fact, the defects are still fade even though their brightness is enhanced compare to the input image. Durand's[25] algorithm seems to have a better local contrast when it comes to enhancing the visibility of the defects and the fine variations of the signal. The output images of Durand's[25] method are slightly more contrasted than those obtained by the other algorithms. However the overall brightness of the image is not enough and in most of the times, Durand's[25] images are dark as the local details are not contrasted enough. This keeps the inspection of the workpieces a bit tedious. The 6-th column (at the top right) shows how the proposed defects visibility enhancement framework effectively highlights the fine variation structures of the signal including the defects and threads without underexposing or overexposing the image. In fact, the combination of the residue with the input image allows us maintain the overall appearance of the image consistent, but the adaptive extraction and amplification of the residual component allows us to better enhance the visibility of defects and threads in NDT & E without being domain or content dependent.

5. CONLUSION

This paper has introduced a framework for defects and threads visibility enhancement in NDT & E based on a "divide and conquer" strategy. we propose to decompose the inspected X-ray images in a way allowing the isolation, and thus the amplification of the defects and threads. The reconstructed image is simply formed as a weighted sum of the original image and the layer containing the meaningful structures. As the image decomposition is mainly controlled by the range parameter of the bilateral filter during the smoothing process, we suggest an automatic selection of the range parameter in order to extend the NDT & E application fields of our method. In this context, we explain how the range parameter that maximizes the TMQI value between the original inspected image and the reconstructed image optimizes the visibility of the defects and threads. The objective and the subjective experiments validate the relevance of our approach, and show that : (i) The proposed range parameter setting is preferred over any reasonable alternative in a large majority of cases. This means that our adaptive method works well for NDT & E images inspection. (ii) The results of our method compare favorably to the ones obtained with existing works destined to visualize High Dynamic Range (HDR) images such as tone-mapping algorithms.

ACKNOWLEDGMENTS

Part of this work has been funded by the 'Pôle Mecatech ADRIC' Walloon Region project, and by the Belgian NSF. Special thanks go to the ISP Group of UCLouvain for the kind and helpful participation to the conducted visual assessment experiments.

REFERENCES

[1] Dong, X., Taylor, C. J., and Cootes, T. F., "Automatic inspection of aerospace welds using x-ray images," in [*2018 24th International Conference on Pattern Recognition (ICPR)*], 2002–2007, IEEE (2018).

[2] Aryan, P., Sampath, S., and Sohn, H., "An overview of non-destructive testing methods for integrated circuit packaging inspection," *Sensors* **18**(7), 1981 (2018).

[3] Ke, C.-Y. and Chen, L.-P., "X-ray inspection for fomcm (fan-out multi chip module) μ-bump non-wet," in [*2021 IEEE 23rd Electronics Packaging Technology Conference (EPTC)*], 93–94, IEEE (2021).

[4] Tao, R., Wei, Y., Jiang, X., Li, H., Qin, H., Wang, J., Ma, Y., Zhang, L., and Liu, X., "Towards real-world x-ray security inspection: A high-quality benchmark and lateral inhibition module for prohibited items detection," in [*Proceedings of the IEEE/CVF International Conference on Computer Vision*], 10923–10932 (2021).

[5] Miao, C., Xie, L., Wan, F., Su, C., Liu, H., Jiao, J., and Ye, Q., "Sixray: A large-scale security inspection x-ray benchmark for prohibited item discovery in overlapping images," in [*Proceedings of the IEEE/CVF Conference on Computer Vision and Pattern Recognition*], 2119–2128 (2019).

[6] Yagoub, B., Ibrahem, H., Salem, A., Suh, J.-W., and Kang, H. S., "X-ray image denoising for cargo dual energy inspection system," in [*2021 International Conference on Electronics, Information, and Communication (ICEIC)*], 1–4, IEEE (2021).

[7] Skurowski, P. and Wicher, K., "High dynamic range in x-ray imaging," in [*International Conference on Information Technologies in Biomedicine*], 39–51, Springer (2018).

[8] Kimpe, T. and Tuytschaever, T., "Increasing the number of gray shades in medical display systems—how much is enough?," *Journal of digital imaging* **20**(4), 422–432 (2007).

[9] Larobina, M. and Murino, L., "Medical image file formats," *Journal of digital imaging* **27**(2), 200–206 (2014).

[10] Wang Rui and Wang Guoyu, "Medical x-ray image enhancement method based on tv-homomorphic filter," in [*2017 2nd International Conference on Image, Vision and Computing (ICIVC)*], 315–318 (2017).

[11] Yeganeh, H. and Wang, Z., "Objective quality assessment of tone-mapped images," *IEEE Transactions on Image Processing* **22**(2), 657–667 (2013).

[12] Huang, Z., Zhang, Y., Li, Q., Li, X., Zhang, T., Sang, N., and Hong, H., "Joint analysis and weighted synthesis sparsity priors for simultaneous denoising and destriping optical remote sensing images," *IEEE Transactions on Geoscience and Remote Sensing* **58**(10), 6958–6982 (2020).

[13] Huang, Z., Wang, Z., Zhang, J., Li, Q., and Shi, Y., "Image enhancement with the preservation of brightness and structures by employing contrast limited dynamic quadri-histogram equalization," *Optik*, 165877 (2020).

[14] Huang, Z., Zhang, Y., Li, Q., Li, Z., Zhang, T., Sang, N., and Xiong, S., "Unidirectional variation and deep cnn denoiser priors for simultaneously destriping and denoising optical remote sensing images," *International Journal of Remote Sensing* **40**(15), 5737–5748 (2019).

[15] Ooi, C. H. and Isa, N. A. M., "Quadrants dynamic histogram equalization for contrast enhancement," *IEEE Transactions on Consumer Electronics* **56**(4), 2552–2559 (2010).

[16] Ooi, C. H. and Isa, N. A. M., "Adaptive contrast enhancement methods with brightness preserving," *IEEE Transactions on Consumer Electronics* **56**(4), 2543–2551 (2010).

[17] Zarie, M., Hajghassem, H., and Majd, A. E., "Contrast enhancement using triple dynamic clipped histogram equalization based on mean or median," *Optik* **175**, 126–137 (2018).

[18] Zeng, M., Li, Y., Meng, Q., Yang, T., and Liu, J., "Improving histogram-based image contrast enhancement using gray-level information histogram with application to x-ray images," *Optik* **123**(6), 511–520 (2012).

[19] Koonsanit, K., Thongvigitmanee, S., Pongnapang, N., and Thajchayapong, P., "Image enhancement on digital x-ray images using n-clahe," in [*2017 10th Biomedical engineering international conference (BME-ICON)*], 1–4, IEEE (2017).

[20] Arici, T. and Altunbasak, Y., "Image local contrast enhancement using adaptive non-linear filters," in [*2006 International Conference on Image Processing*], 2881–2884 (2006).

[21] Goto, T., Ikeyama, M., and Hirano, S., "Contrast enhancement and detailed enhancement method based on non-linear filtering," in [*2018 IEEE International Conference on Consumer Electronics-Taiwan (ICCE-TW)*], 1–5 (2018).

[22] Lu, Z., Long, B., Li, K., and Lu, F., "Effective guided image filtering for contrast enhancement," *IEEE Signal Processing Letters* **25**(10), 1585–1589 (2018).

[23] Yue, Z. Q. and Morin, I., "Digital image processing for aggregate orientation in asphalt concrete mixtures," *Canadian Journal of Civil Engineering* **23**(2), 480–489 (1996).

[24] Perona, P. and Malik, J., "Scale-space and edge detection using anisotropic diffusion," *IEEE Transactions on pattern analysis and machine intelligence* **12**(7), 629–639 (1990).

[25] Durand, F. and Dorsey, J., "Fast bilateral filtering for the display of high-dynamic-range images," in [*ACM transactions on graphics (TOG)*], **21**(3), 257–266, ACM (2002).

[26] Petschnigg, G., Szeliski, R., Agrawala, M., Cohen, M., Hoppe, H., and Toyama, K., "Digital photography with flash and no-flash image pairs," in [*ACM transactions on graphics (TOG)*], **23**(3), 664–672, ACM (2004).

[27] Madmad, T. and De Vleeschouwer, C., "Bilateral histogram equalization for x-ray image tone mapping," in [*2019 IEEE International Conference on Image Processing (ICIP)*], 3507–3511, IEEE (2019).

[28] He, K., Sun, J., and Tang, X., "Guided image filtering," *IEEE transactions on pattern analysis and machine intelligence* **35**(6), 1397–1409 (2012).

[29] M. J., F., J, S., J., B., and Y., M., "Image decomposition and separation using sparse representations: An overview," *Proceedings of the IEEE* **98**(6), 983–994 (2010).

[30] Madmad, T., Delinte, N., and De Vleeschouwer, C., "Cnn-based morphological decomposition of x-ray images for details and defects contrast enhancement," in [*Proceedings of the IEEE/CVF Conference on Computer Vision and Pattern Recognition*], 2170–2180 (2021).

[31] He, K., Sun, J., and Tang, X., "Guided image filtering," in [*European conference on computer vision*], 1–14, Springer (2010).

[32] Eisemann, E. and Durand, F., "Flash photography enhancement via intrinsic relighting," in [*ACM transactions on graphics (TOG)*], **23**(3), 673–678, ACM (2004).

[33] Paris, S., Kornprobst, P., Tumblin, J., and Durand, F., [*Bilateral filtering: Theory and applications*], Now Publishers Inc (2009).

[34] Wang, Z., Simoncelli, E. P., and Bovik, A. C., "Multiscale structural similarity for image quality assessment," in [*The Thrity-Seventh Asilomar Conference on Signals, Systems & Computers, 2003*], **2**, 1398–1402, Ieee (2003).

[35] Geisler, W. S., "Visual perception and the statistical properties of natural scenes," *Annu. Rev. Psychol.* **59**, 167–192 (2008).

[36] Yeganeh, H. and Wang, Z., "Objective quality assessment of tone-mapped images," *IEEE Transactions on Image processing* **22**(2), 657–667 (2012).

[37] Farbman, Z., Fattal, R., Lischinski, D., and Szeliski, R., "Edge-preserving decompositions for multi-scale tone and detail manipulation," in [*ACM Transactions on Graphics (TOG)*], **27**(3), 67, ACM (2008).

[38] Ashikhmin, M. and Goyal, J., "A reality check for tone-mapping operators," *ACM Transactions on Applied Perception (TAP)* **3**(4), 399–411 (2006).

[39] Reinhard, E. and Devlin, K., "Dynamic range reduction inspired by photoreceptor physiology," *IEEE Transactions on Visualization & Computer Graphics* (1), 13–24 (2005).

[40] Zhang, L., Zhang, L., Mou, X., and Zhang, D., "Fsim: A feature similarity index for image quality assessment," *IEEE transactions on Image Processing* **20**(8), 2378–2386 (2011).